Report D4.1 (M9)

Title of the project	Enhanced safety materials for Li-ion batteries
Short title	ENSAMAT
TRL:	1-3
Code:	09I04-03-V02-00028
Beginning of the project:	1.1.2025
Duration:	20 months

Deliverable number	**Deliverable**	**Work package code**	**Entity responsible for deliverable**	**Type**	**Access and dissemination**	**Method of verification**	**Delivery (project implementation month)**
D4.1	Properties of selected electrodes and batteries	WP4	SUT	Report	P	Experimental results	M9

Report M1-M12 (D4.1)

This output focuses on the properties of selected electrodes and batteries, with special emphasis on their structure, morphology and electrochemical behavior. The aim is to provide a basis for understanding the relationship between material characteristics and cell performance through systematic characterization. The work is carried out within task 4.1 (Structural, morphological and electrochemical characterization) and task 4.2 (Advanced electrical and electrochemical characterization). Structural and morphological analysis is combined with electrochemical methods to assess the electrode-electrolyte interfaces, as well as transport and kinetic processes during cycling. Advanced techniques such as electrochemical impedance spectroscopy (EIS) and galvanostatic intermittent titration technique (GITT) are used to evaluate ion diffusion, charge transfer processes and overall electrochemical response of selected half-cell and full-cell cells. In addition, impedance data are analyzed using an electrical surrogate model (ECM), which allows obtaining key electrical parameters describing the investigated batteries. The results provide fundamental knowledge necessary for a deeper understanding of the investigated electrochemical systems and form the basis for further tasks of the project.

Task 4.1 (Structural, morphological and electrochemical characterization)

Stabilization of the SEI layer and improvement of the performance of SiG anodes using ALD ZnO layers

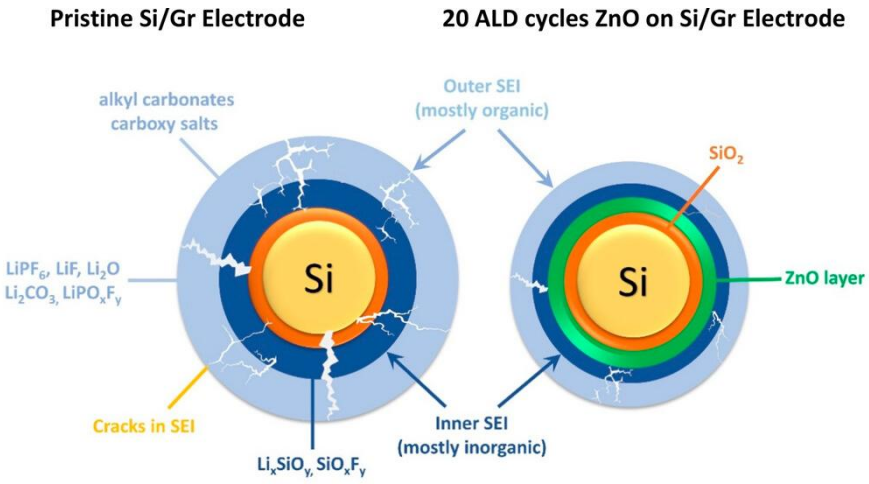


Figure 1. Schematic representation of the SEI layer and its components for the original electrodes and for 20 ALD cycles of ZnO on Si/Gr electrodes.

Silicon (Si) is a promising anode material due to its high theoretical capacity. It is also the second most abundant element in the Earth's crust. However, the formation of an unstable solid electrolyte interlayer (SEI) and significant volume expansion during lithiation cause structural degradation, which leads to capacity loss and limits the cyclic life of silicon-based anodes.

In this study, the electrochemical performance of silicon/graphite (Si/Gr) composite electrodes was investigated after modification with nanometer-thick ZnO films deposited by atomic layer deposition (ALD). The ZnO layers were deposited in a range of 5–40 ALD cycles on approximately 20 µm thick Si/Gr electrodes.

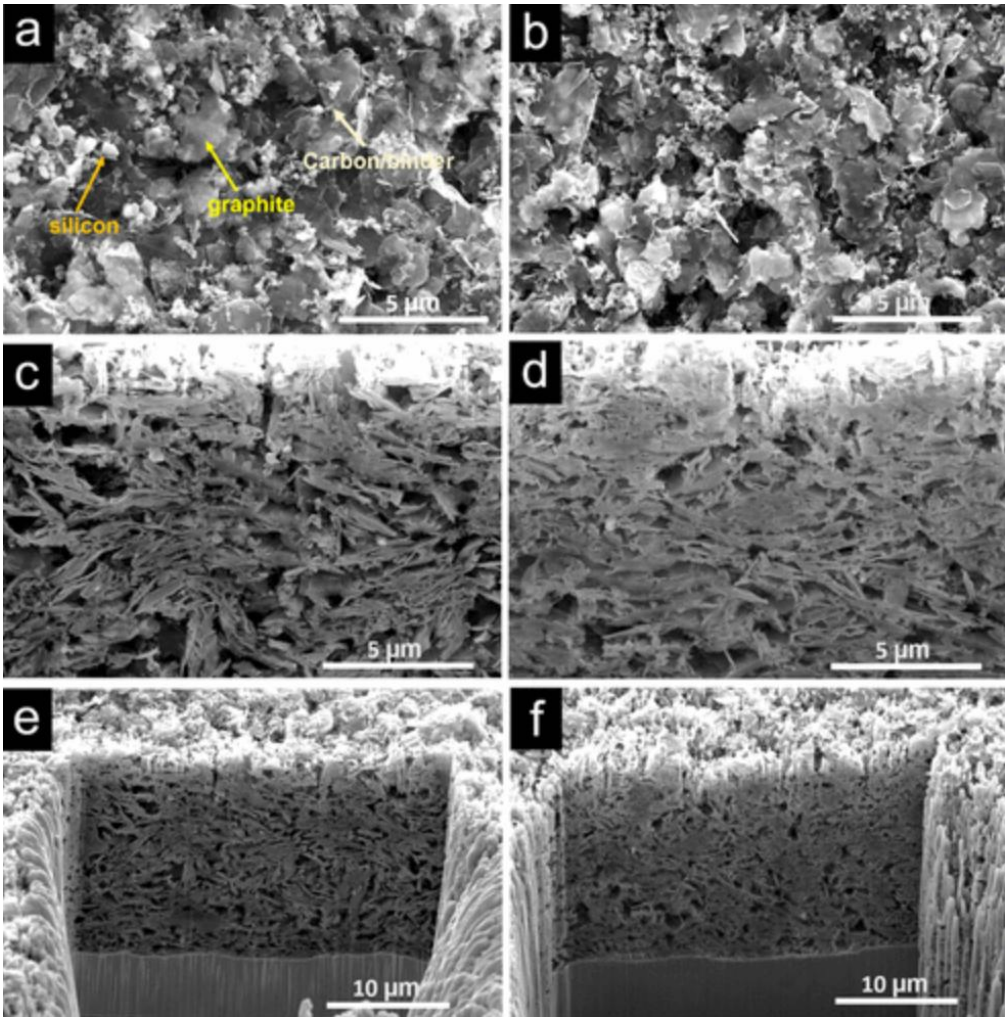


Figure 2. SEM images from above for (a) pristine and (b) 20 ALD cycles of ZnO on Si/Gr electrodes. Cross-sections of (c and e) pristine and (d and f) 20 ALD cycles of ZnO on Si/Gr electrodes before electrochemical testing.

Electrochemical characterization included galvanostatic cycling at various C-rates and EIS in half-cell configuration, while structural and chemical changes were investigated by scanning electron microscopy (SEM) and X-ray photoelectron spectroscopy (XPS) before and after electrochemical cycling. The ZnO-coated electrodes clearly demonstrated improved performance at higher current loads compared to the original Si/Gr electrodes. The reversible conversion of ZnO ALD films during lithiation/delithiation was confirmed by dQ/dV analysis and XPS, indicating that the ultrathin ZnO layers act as a protective coating, passivate the electrode surface, help form a more stable SEI layer, and facilitate Li-ion transport across the interface. Comparison of pristine and ZnO-modified samples revealed significant differences in the (de)lithiation mechanisms. Electrodes with 20 ALD cycles of ZnO showed the optimal layer thickness and the best performance of all tested samples. At C-rate 2, a larger part of

the electrode remained electrochemically accessible in the case of the ZnO layer, allowing for more complete lithiation. EIS measurements confirmed significantly reduced SEI and charge transfer resistance in ZnO-coated electrodes, with these low resistance values being maintained for at least 100 cycles at C-rate 1. XPS analysis further showed that ZnO modification affects the composition of the SEI layer. While both pristine and coated electrodes formed SEI layers containing typical compounds such as Li_2CO_3, LiF, $LiPF_6$/LixPOyFz, alkyl carbonates and carboxylate salts, the pristine samples showed increased carbonate formation after cycling. In contrast, ZnO-coated electrodes limited carbonate accumulation and maintained a thinner and more stable SEI layer.

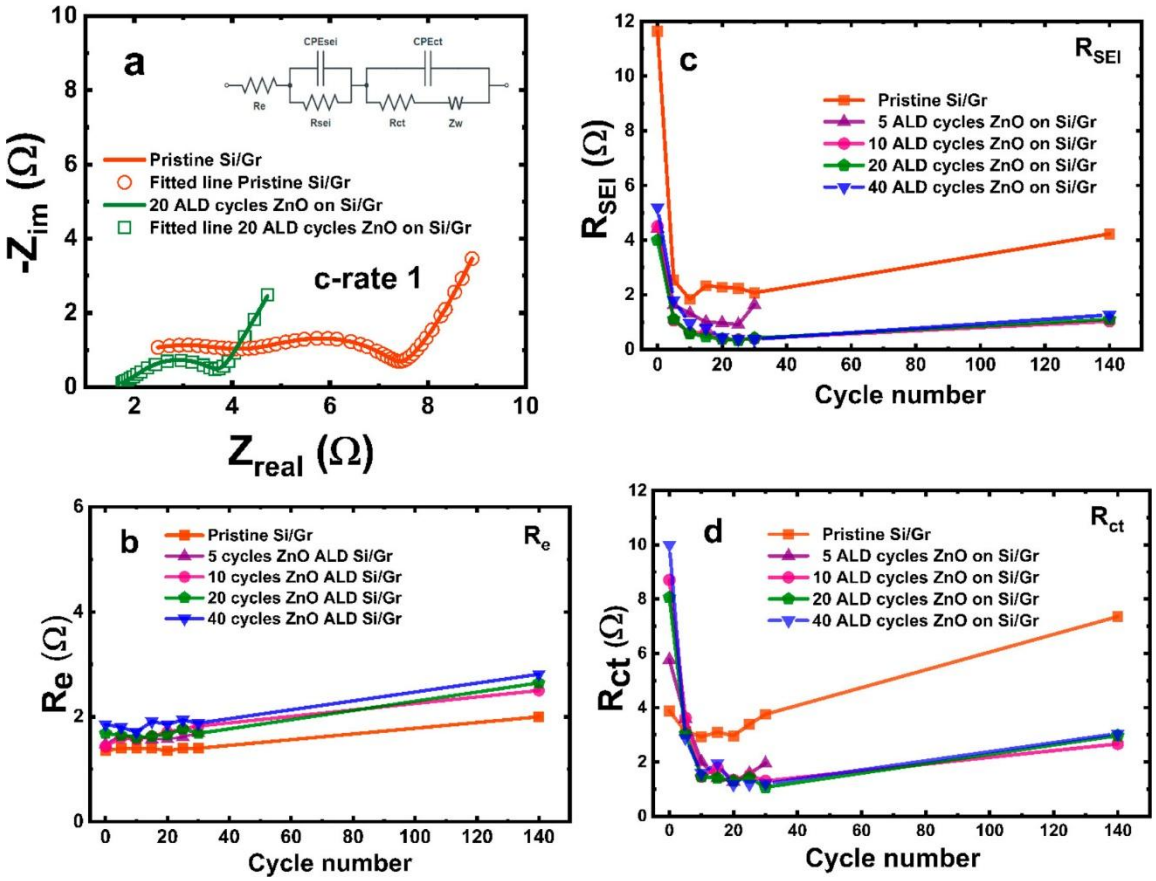


Figure 3. Nyquist plot of pristine and 20 ALD cycles of ZnO on Si/Gr anodes obtained after discharge/charge cycles at 1 C (a). Inset: ECM model used for curve fitting. Re (b), RSEI (c) and Rct (d) values obtained by curve fitting of EIS spectra.

These results confirm that the ZnO layer deposited by ALD plays a protective and stabilizing role. It reduces the interface resistance, improves Li-ion transport, and significantly increases the ability of the electrodes to operate at higher current loads. Since ZnO is a cheap and widely available material, the application of nanometric ZnO layers by ALD can be considered an effective and scalable approach to improve the performance and lifetime of silicon-based anodes.

Improved performance of $LiFePO_4$ cathodes with Al nanolayer deposited by ALD: insights from electrochemical analysis, operando X-ray diffraction and X-ray photoelectron spectroscopy

This study investigated the effect of ultrathin Al_2O_3 (aluminum oxide) layers deposited by atomic layer deposition (ALD) on the electrochemical performance of $LiFePO_4$ (LFP) cathodes in lithium-ion batteries. ALD layers in the range of 2–20 cycles were applied to LFP electrodes and their effect on the capability of working at different current loads, cycling stability and electrode/electrolyte interface behavior was systematically investigated.

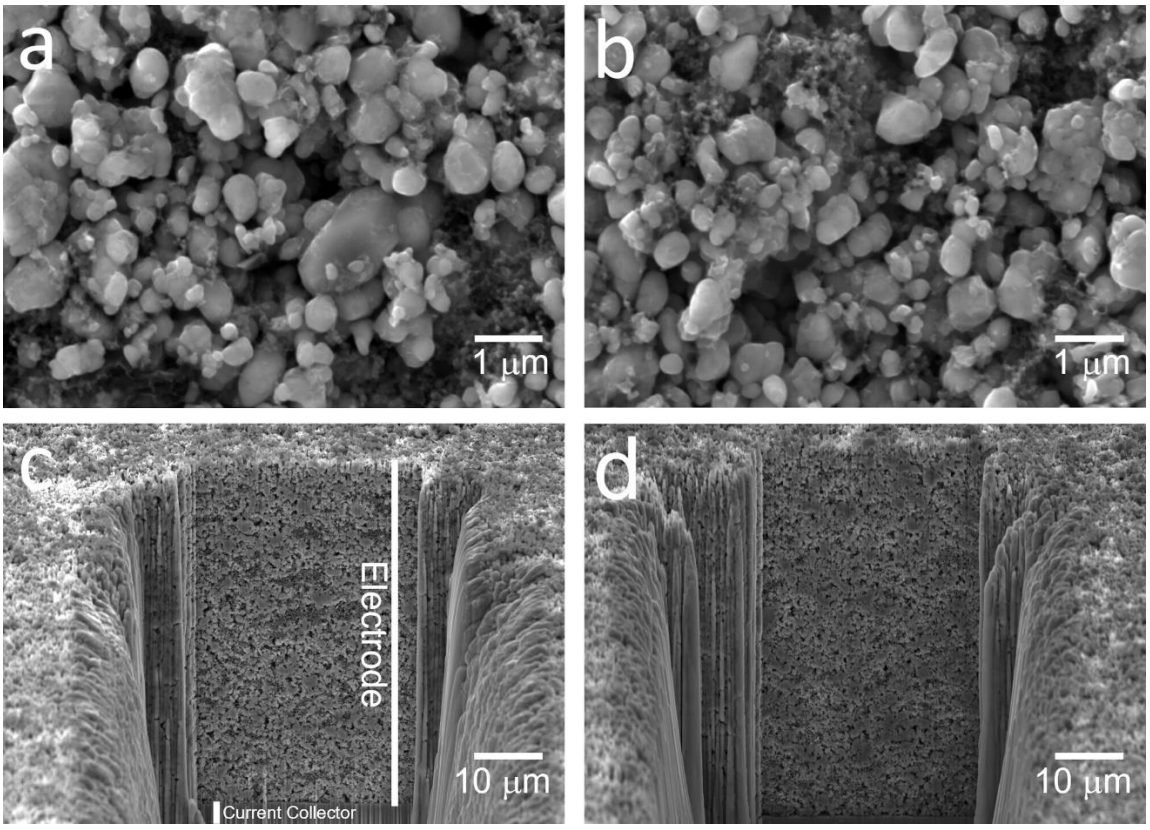


Figure 4. SEM top views of (a) pristine and (b) 5 ALD cycles alumina on $LiFePO_4$ electrodes. Cross-sections of (c) pristine and (d) 5 ALD cycles alumina on $LiFePO_4$ electrodes before electrochemical testing.

Electrochemical tests, including cyclic voltammetry (CV), galvanostatic charge–discharge (GCD), and electrochemical impedance spectroscopy (EIS), were performed on both pristine and ALD-coated samples. Cathodes with 5–10 ALD cycles showed the best performance, achieving significantly improved discharge capacities at higher C-rates (1–2 C) compared to uncoated electrodes. These results confirm that the ultrathin Al_2O_3 layers act as effective protective barriers, reducing direct electrolyte contact and thereby mitigating structural degradation of the cathode surface.

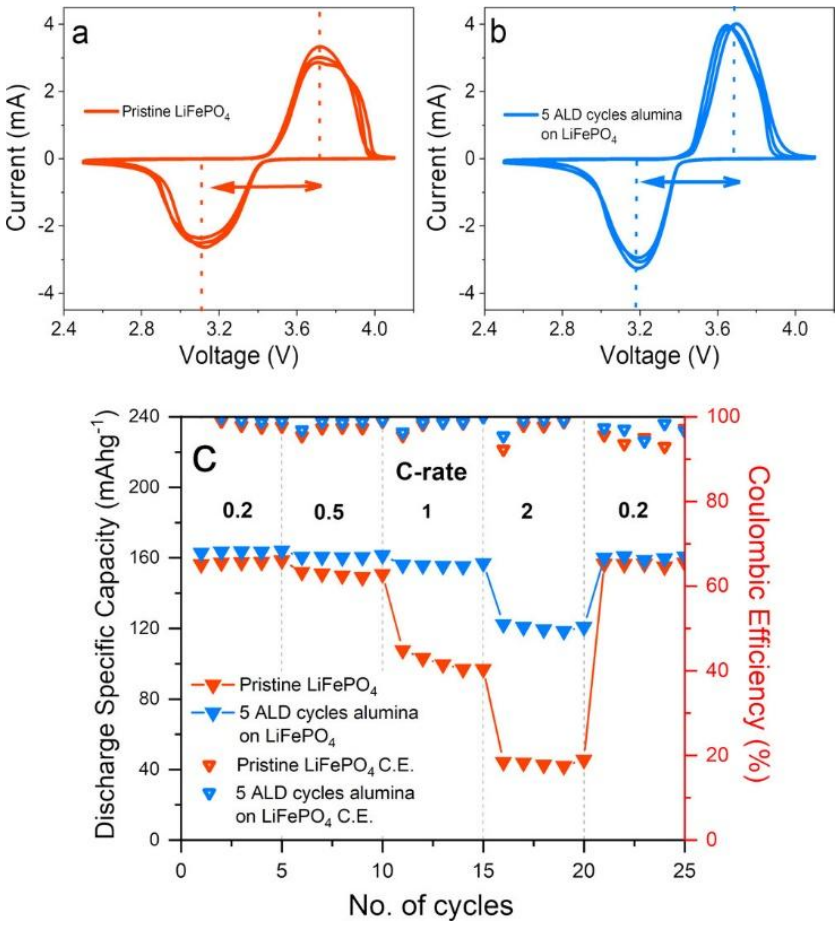


Figure 5. Cyclic voltammograms of (a) pristine and (b) $LiFePO_4$ with 5 ALD cycles of Al_2O_3 at a scan rate of 0.1 $mV \cdot s^{-1}$ in the potential range of 2.5–4.1 V. Dashed lines and arrows indicate the positions of oxidation/reduction peaks and polarization. (c) Cyclic performance of pristine $LiFePO_4$ and $LiFePO_4$ with 5 Al_2O_3 cycles at different C-rates in half-cell configuration.

Impedance analysis showed that Al_2O_3-coated samples exhibited lower charge transfer resistance and reduced CEI (parasitic interface at the cathode) resistance compared to the pristine electrodes. This suggests that the ALD Al_2O_3 layers facilitate Li-ion transport across the interface and contribute to more stable electrochemical kinetics. Operando X-ray diffraction (XRD) measurements confirmed that the $LiFePO_4 \rightarrow FePO_4$ phase transition during cycling was more reversible in the coated electrodes, highlighting the protective role of the Al_2O_3 film. X-ray photoelectron spectroscopy (XPS) analysis further supported these findings. Both pristine and coated electrodes exhibited compounds such as Li_2CO_3 and LiF in the SEI/CEI layer; however, an increased LiF content was observed in the coated samples after cycling, consistent with improved passivation. Importantly, the Al_2O_3 layer remained detectable even after 100 cycles at a C-rate of 1, demonstrating the robustness and long-term stability of the ALD-deposited layers.

Ultrathin Al_2O_3 layers deposited by ALD provide a scalable and efficient way to improve the performance of $LiFePO_4$ cathodes. By stabilizing the CEI, reducing interface resistance, and maintaining structural integrity, the coated cathodes achieve improved higher current capability and longer cycle life compared to native LFP electrodes.

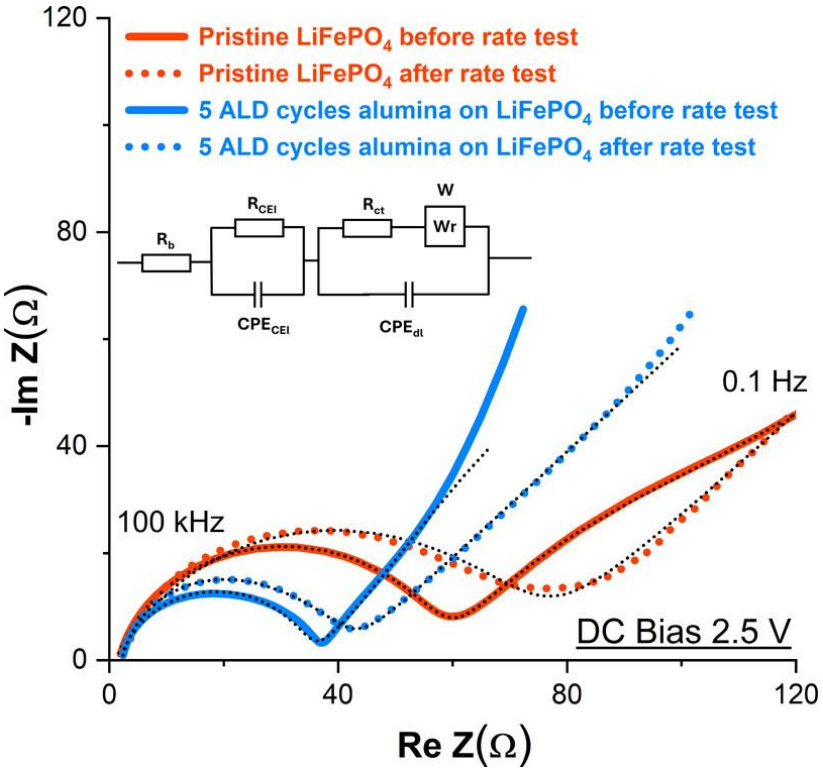


Figure 6. Nyquist plot of the pristine and 5 ALD cycles Al_2O_3 coated $LiFePO_4$ cathode obtained before and after the current load test. The short dashed lines show the fit of the experimental data using the equivalent circuit shown in the inset.

Task 4.2 (Advanced electrical and electrochemical characterization)

In-situ EIS for corrosion detection in Li-ion batteries with LiFSI electrolyte

LiFSI-based electrolytes are considered attractive candidates for the next generation of high-voltage and high-temperature Li-ion batteries. However, their main drawback is their tendency to corrode aluminum (Al) current collectors. Understanding and suppressing this corrosion is crucial for the safe and reliable operation of Li-ion cells with such electrolytes. In this work, in-situ EIS was used to detect corrosion of the aluminum current collector in NMC622/graphite cells containing 1.0 M LiFSI in EC:DMC (1:1, v/v). Cells cycled to 4.2 V at 50 °C exhibited characteristic induction loops in the Nyquist plots on the cathode side, which were attributed to aluminum corrosion. The presence of corrosion was further confirmed by scanning electron microscopy, which showed corrosive damage to the aluminum surface. A battery surrogate electrical model was proposed to describe the evolution of this phenomenon during cycling. When the upper voltage limit was reduced to 3.7 V, corrosion was successfully suppressed. Under these conditions, Nyquist plots showed no induction loops and SEM imaging revealed no signs of corrosion, confirming that the protective native Al_2O_3 layer was preserved. This direct correlation between EIS response and Al corrosion points to the diagnostic potential of EIS as an in-situ tool for assessing electrolyte-induced degradation processes.

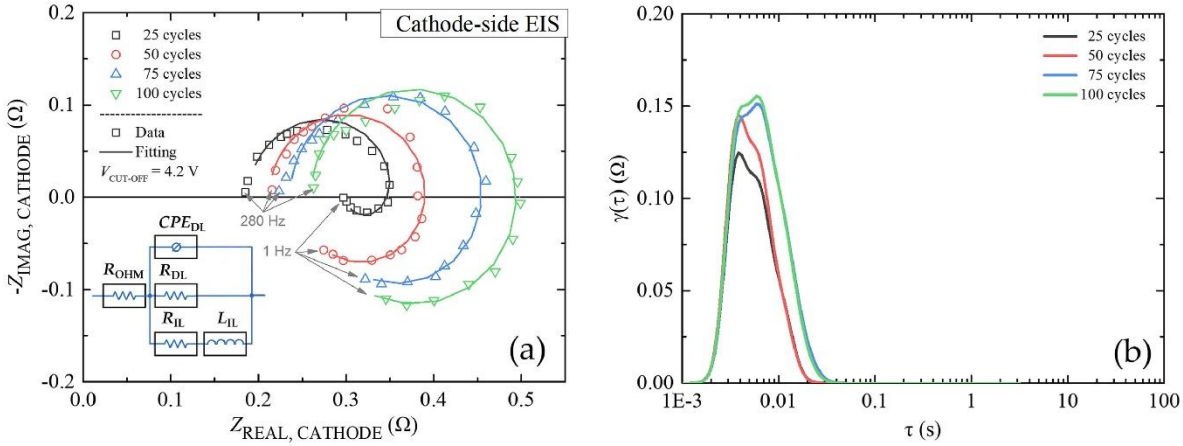


Figure 7. (a) Nyquist plots and (b) DRT of the cathode of a cell cycled to 4.2 V.

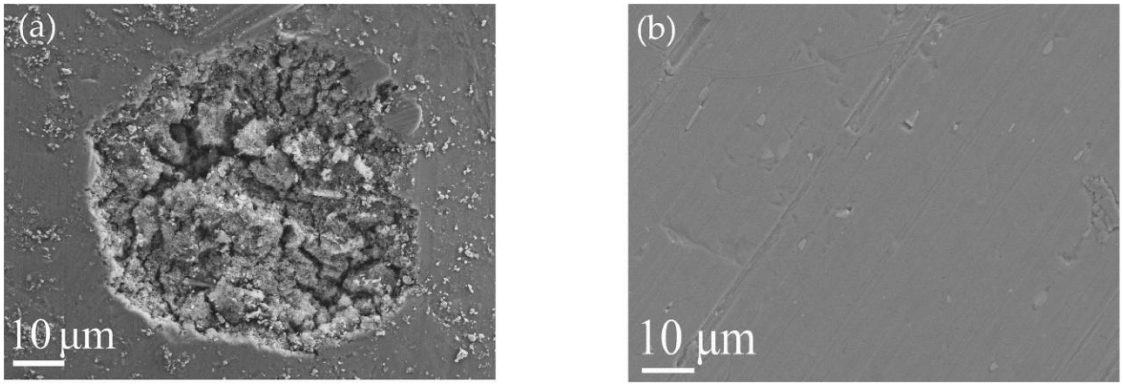


Figure 8. SEM images of aluminum current collectors taken from cells tested for 100 cycles with an upper voltage limit of (a) 4.2 V and (b) 3.7 V.

The study shows that LiFSI-based electrolytes can cause corrosion of aluminum current collectors at elevated temperatures and voltages, but such effects can be mitigated by limiting the voltage. These results contribute to the design of high-voltage LiFSI-based electrolytes by providing a methodology for real-time corrosion detection and offering insights into strategies for its suppression.

Electrochemical characterization of thermal properties of ZnO coated SiG anodes – preliminary results

EIS measurements were performed on experimental Si/Gr half-cell cells with an ALD-deposited ZnO protective layer, assembled in a PAT-Cell configuration. Metallic lithium was used as the anode. Measurements were performed at different temperatures (15 °C, 25 °C, 35 °C and 45 °C). The cells were charged sequentially from a fully discharged state to 1.4 V in steps of 0.1 V. After each charging step, the cells were allowed to relax for 5 h before performing EIS measurements. Impedance spectra were fitted with a surrogate electrical model and the evolution of R_{OHM}, R_{DL}, R_{CHT} and Warburg element as a function of state of charge (SOC) and temperature was evaluated.

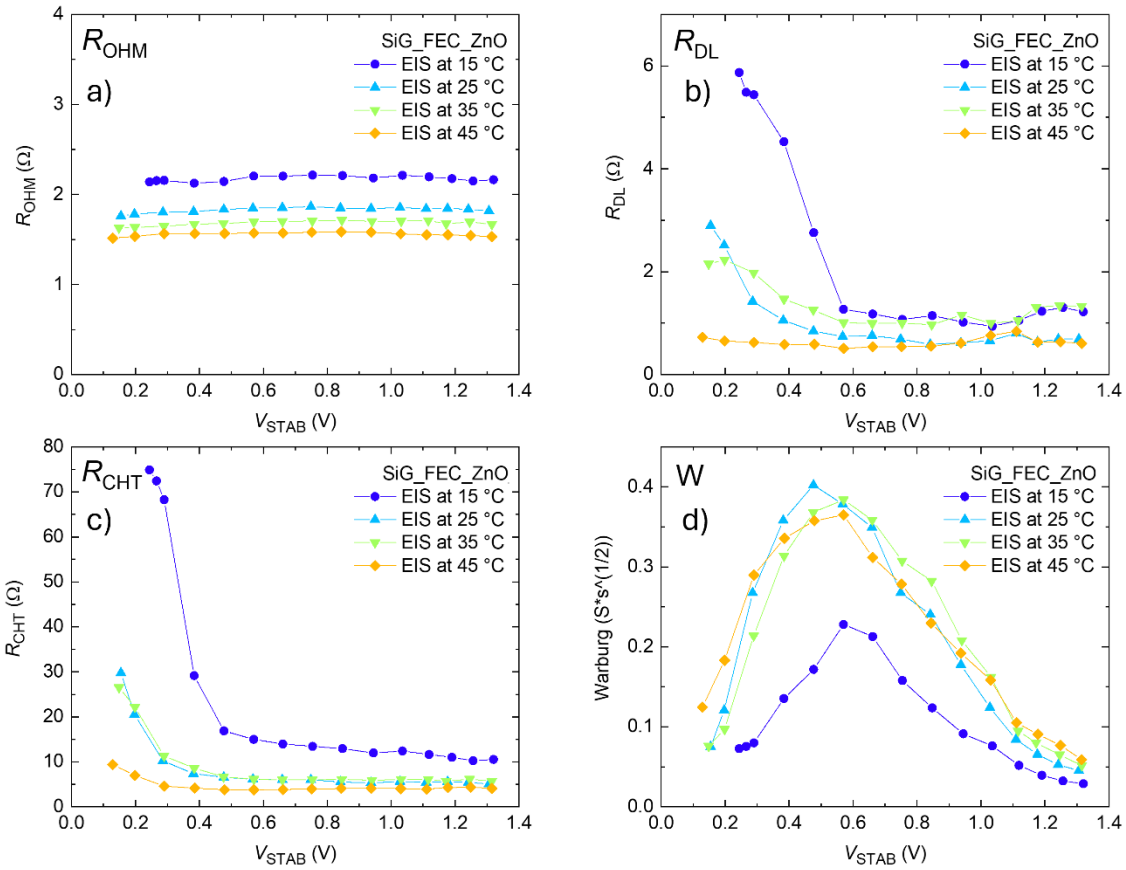


Figure 9. Results of fitting EIS data using a surrogate electrical model, measured at different temperatures and states of charge of an experimental ZnO-coated SiG half-cell battery.

- **R_{OHM}** The ohmic resistance remained almost constant across all SOC and temperature conditions, indicating stable electrolyte and contact resistances.

- **R_{DL}** The double layer resistance showed increasing values with decreasing temperature, with this effect being most pronounced at lower voltages.

- **R_{CHT}** The charge transfer resistance was relatively stable in the range of 0.6 V to 1.4 V. However, below 0.6 V Rct increased significantly as the potential approached 0 V, with this effect being more pronounced at lower temperatures.

- **W** The diffusion-related impedance showed a peak-shaped profile with a maximum around 0.5 V and decreasing values towards both higher and lower voltage extremes. At 25, 35 and 45 °C the Warburg constant had comparable values, while at 12 °C it decreased significantly, indicating limited Li-ion diffusion at reduced temperature.

These preliminary results confirm the strong dependence of interface and transport processes on both voltage and temperature in ZnO-doped Si/Gr electrodes. The observed increase in RDL and RCHT at low temperatures and low voltages, together with the suppressed diffusion processes at 12 °C, highlight the importance of extending the study to 0 °C and lower temperatures to fully capture the performance limitations under realistic operating conditions.

Effect of operating window on degradation and OCV behavior of SiOx/graphite anodes – preliminary results

In this part of the study, commercially available Molicel M35A 18650 cells (nominal capacity 3.5 Ah) were investigated. The electrodes of these cells consist of composite materials: the anode is composed of approximately 87 wt% graphite, approximately 10 wt% silicon dioxide (SiOx), and approximately 3 wt% inactive components, while the cathode is composed of approximately 93 wt% nickel-cobalt-aluminum oxide (NCA) and approximately 7 wt% inactive components. The presence of SiOx in the anode composite makes these cells particularly suitable for analyzing how silicon degradation affects the open circuit voltage (OCV) behavior during cycling. The primary objective was to evaluate how cycling in different state of charge (SOC) windows affects degradation and the subsequent evolution of the OCV curve. Since the silicon fraction in composite anodes tends to degrade most significantly at low SOC, three cycling scenarios were implemented:

- o Cycling within a low SOC window
- o Cycling within a high SOC window
- o Cycling within the entire SOC window

The capacity decay, converted to equivalent full cycles, clearly showed that cycling in the low SOC window led to the fastest degradation. After approximately 300 cycles, the cells in this scenario completely failed. In contrast, cycling in the entire SOC window showed a gradual capacity decay without failure, while cycling in the high SOC window showed only a minimal capacity decay, indicating that degradation processes are significantly suppressed in this scenario.

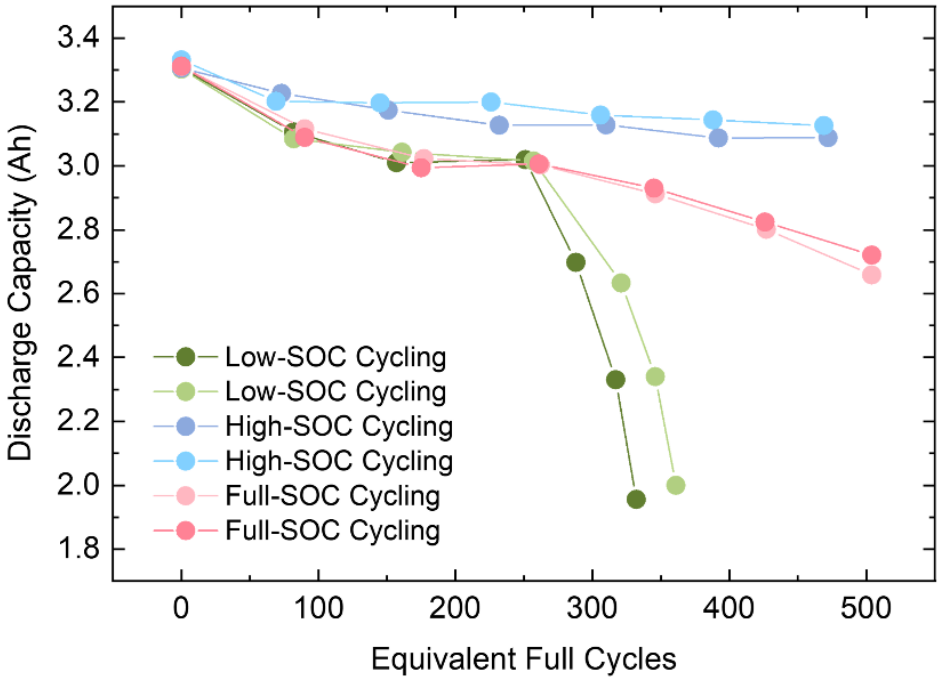


Figure 10. Evolution of discharge capacities of commercial Li-ion batteries with SiG anodes cycled in different SOC window ranges.

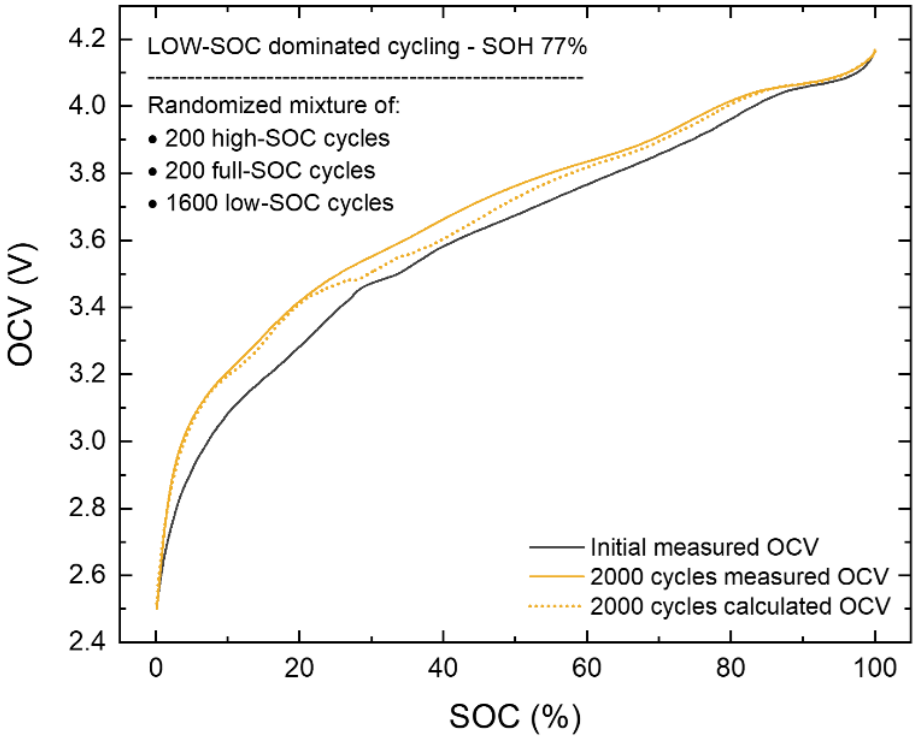


Figure 11. Selected comparison of measured and calculated OCV curve with the OCV curve obtained during initialization of a new battery.

To further investigate the effect of cycling history, OCV curves were measured after defined cycle intervals: every 100 cycles when cycling in the full SOC window and every 400 cycles when cycling in the low and high SOC windows (to ensure comparable EFC numbers between scenarios). The OCV curves revealed significant shifts depending on the cycling window, confirming that the degradation of the silicon fraction changes the behavior of the composite electrode and thus the overall voltage profile. In the second part of the experiment, the cells were cycled in combined SOC windows. The OCV curve was reconstructed using degradation data from individual cycling scenarios, combined according to the cycling history (SOC window ratios). Several scenarios were tested, including 1:1:1, 8:1:1, 1:8:1, and 1:1:8 ratios, as well as completely random cycling scenarios. The reconstructed OCV curves showed visual agreement with the experimentally measured OCV curves of cells degraded under the corresponding combined conditions. This demonstrates that the OCV curve of degraded cells with composite anodes can be approximated by weighting the degradation contributions from different SOC windows.

Several scenarios were tested, including 1:1:1, 8:1:1, 1:8:1, and 1:1:8 ratios, as well as completely random cycling scenarios. The reconstructed OCV curves showed visual agreement with the experimentally measured OCV curves of cells degraded under the corresponding combined conditions. This demonstrates that the OCV curve of degraded cells with composite anodes can be approximated by weighting the degradation contributions from different SOC windows.

These findings are crucial for battery management systems (BMS), as the OCV–SOC relationship changes as silicon-containing composite anodes degrade. If the OCV curve is not

updated over the battery life, the SOC estimate may become inaccurate. The presented methodology offers a way to dynamically generate and update OCV curves based on the actual cell cycling history, thereby enabling more accurate SOC determination in the BMS and supporting safer and more reliable operation of lithium-ion batteries with Si/Gr composite anodes.

Effect of ambient temperature on electrochemical properties of silicon-rich Gr/Si composite electrode for advanced Li-ion batteries – preliminary results

This ongoing experiment focuses on half-cell batteries using lithium metal as the reference electrode and a composite electrode as the working electrode. In this composite, conventional graphite is partially replaced by a high-silicon material, which constitutes approximately 50% of the total electrode weight. The electrolyte formulation contains fluoroethylene carbonate (FEC) as an additive to improve the stability of the SEI layer. EIS measurements were performed over the full potential range of the half-cell cell (0–1.5 V vs. Li/Li^+). The protocol consisted of a full discharge followed by a 1-hour relaxation to reach the cell equilibrium state, after which the EIS spectrum was recorded. The cell was then charged in 0.1 V steps, with each step followed by a 1-hour relaxation and subsequent EIS measurement. This procedure was repeated until 1.5 V was reached, where the final relaxation and EIS measurement were performed. The OCV measured after each relaxation step was used as a reference for all graphical representations.

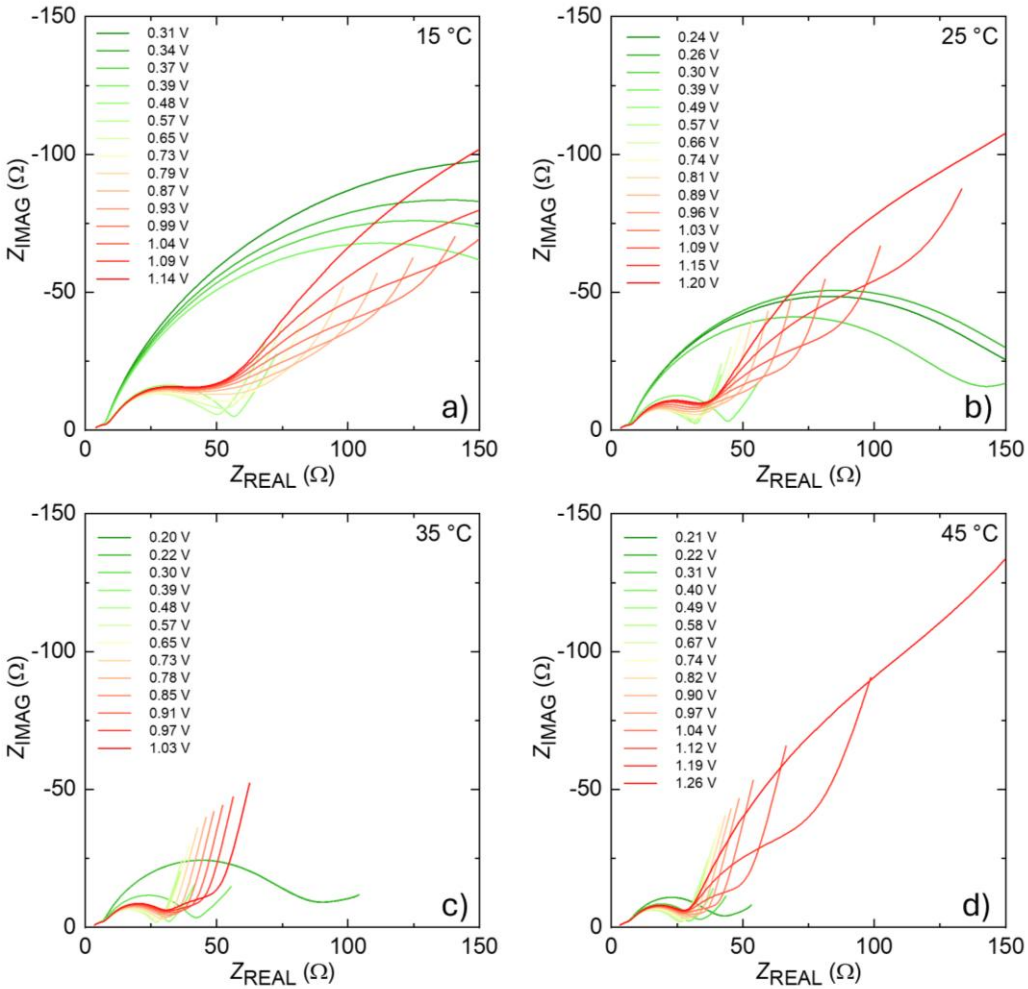


Figure 12. Nyquist plots of the investigated half-cell battery obtained at different OCV levels and different temperatures, where a) represents measurements at 15 °C, b) at 25 °C, c) at 35 °C, and d) at 45 °C.

The experiment was repeated at four different temperatures: 15 °C, 25 °C, 35 °C and 45 °C. The resulting Nyquist plots are shown in Figure 12, where a) – d) correspond to measurements at 15 °C, 25 °C, 35 °C and 45 °C. At the lowest OCV values, the impedance spectra show very large real and imaginary impedance components, creating a prominent high-frequency semicircle, indicating a strong polarization of the electrode–electrolyte interface. As the cell potential increases, this polarization effect weakens, followed by a gradual increase in the diameter of the dominant semicircle with increasing SOC (represented by the OCV values). In all temperature regimes, the appearance of a second semicircle is observed at lower frequencies, which becomes clearly visible for OCV values above approximately 1 V. As expected, EIS spectra measured at lower temperatures generally show higher impedance values. In addition, a temperature-dependent shift in the onset of the second semicircle was observed, suggesting that the interface kinetics and diffusion processes are affected by temperature in a different way. Future work will include the analysis of these measurements using the Distributed Relaxation Time (DRT) method of simulation with a surrogate electrical model. These results will be compared with measurements performed on electrodes with different graphite to silicon ratios to elucidate the influence of silicon content on the impedance behavior.

Summary of results presented in Report M1-M12 (D4.1)

The work presented in this report focuses on the systematic structural, morphological and electrochemical characterization of selected electrodes and batteries with the aim of better understanding the relationship between material properties and cell performance. In tasks 4.1 and 4.2, experiments combining microscopic and spectroscopic techniques with electrochemical methods were performed.

- Si/Gr anodes with ALD ZnO layers demonstrated the protective and stabilizing function of ultrathin ZnO layers. ZnO reduced the resistance of the SEI layer and improved Li-ion transport. The best performance was shown by electrodes with 20 ALD cycles, while the low charge transfer resistance was maintained for at least 100 cycles.
- $LiFePO_4$ cathodes with ALD Al_2O_3 layers showed improved performance at high C-rates, lower CEI interface resistance and more stable cycling life. Operando XRD and XPS confirmed a more reversible phase transition and better passivation of the investigated surface.
- In-situ EIS measurements allowed to detect corrosion of the aluminum current collector in experimental half-cells with LiFSI electrolyte. At 50 °C and 4.2 V, characteristic induction loops appeared, which were not present in the Nyquist plots after lowering the voltage limit to 3.7 V, confirming the diagnostic potential of EIS for monitoring corrosion degradation of current collectors.
- Preliminary EIS results on ZnO/SiGr half-cell anodes showed stable ohmic resistance, increase of double layer resistance and charge transfer at low temperatures and low SOC, and suppressed lithium ion diffusion at 15 °C.
- The impact of different SOC windows on the degradation of SiOx/graphite anodes and the evolution of OCV curves was analyzed for commercial Molicel M35A cells. A methodology was developed to reconstruct OCV curves based on cycling history, which is important for more accurate SOC estimation in BMS systems.